HHS Public Access

Author manuscript

*ACS Biomater Sci Eng*. Author manuscript; available in PMC 2022 June 14.

Published in final edited form as:

*ACS Biomater Sci Eng*. 2021 June 14; 7(6): 2430–2443. doi:10.1021/acsbiomaterials.0c01803.

# Collagen I Fibrous Substrates Modulate the Proliferation and Secretome of Estrogen Receptor-Positive Breast Tumor Cells in a Hormone-Restricted Microenvironment

**Ana M. Reyes-Ramos**,
Department of Chemical Engineering, University of Puerto Rico—Mayagüez, Mayagüez, Puerto Rico 00681-9000, United States

**Yasmín R. Álvarez-García**,
Department of Chemistry, University of Wisconsin—Madison, Madison, Wisconsin 53706, United States

**Natalia Solodin**,
Department of Oncology, McArdle Laboratories for Cancer Research and University of Wisconsin Carbone Comprehensive Cancer Center, University of Wisconsin—Madison, Madison, Wisconsin 53705, United States

**Jorge Almodovar**,
Ralph E. Martin Department of Chemical Engineering, University of Arkansas, Fayetteville, Arkansas 72701, United States

**Elaine T. Alarid**,
Department of Oncology, McArdle Laboratories for Cancer Research and University of Wisconsin Carbone Comprehensive Cancer Center, University of Wisconsin—Madison, Madison, Wisconsin 53705, United States

**Wandaliz Torres-Garcia**,
Department of Industrial Engineering, University of Puerto Rico—Mayagüez, Mayagüez, Puerto Rico 00681-9000, United States

**Maribella Domenech**
Department of Chemical Engineering, University of Puerto Rico—Mayagüez, Mayagüez, Puerto Rico 00681-9000, United States

**Corresponding Author: Maribella Domenech –** Department of Chemical Engineering, University of Puerto Rico—Mayagüez, Mayagüez, Puerto Rico 00681-9000, United States; maribella.domenech@upr.edu.

Author Contributions

This work was accomplished with the support from NIH-NCI 1K01CA188167, Puerto Rico Science, Technology & Research Trust (#2016-00064B) and partial support from the Engineering Research Center for Cell Manufacture Technologies funded by the National Science Foundation under Grant No. EEC-1648035.

Supporting Information

The Supporting Information is available free of charge at https://pubs.acs.org/doi/10.1021/acsbiomaterials.0c01803.
Figures of complete images of the fiber organization on the substrate surface, ER signaling in MCF-7 cells cultured in different collagen fibers diameter, ER transactivation of MCF-7 MVLN cells, representative fluorescent images of MCF-7 and T-47D cells stained with Hoechst, ER signaling and resistance to ER inhibitors in T-47D cells, and table of secretome profile of 640 human factors of MCF-7 and T-47D cells cultured on different substrates (PDF)

Complete contact information is available at: https://pubs.acs.org/10.1021/acsbiomaterials.0c01803

The authors declare no competing financial interest.

## Abstract

The fibril orientation of type I collagen has been shown to contribute to tumor invasion and metabolic changes. Yet, there is limited information about its impact on tumor cells' behavior in a restrictive growth environment. Restrictive growth environments are generated by the inhibition of a proliferation stimulus during therapy or as an inflammatory response to suppress tumor expansion. In this study, the impact of a type I collagen matrix orientation and fibrous architecture on cell proliferation and response to estrogen receptor (ER) therapy were examined using estrogen-dependent breast tumor cells (MCF-7 and T-47D) cultured in a hormone-restricted environment. The use of hormone-free culture media, as well as pharmacological inhibitors of ER, Tamoxifen, and Fulvestrant, were investigated as hormone restrictive conditions. Examination of cultures at 72 h showed that tumor cell proliferation was significantly stimulated (1.8-fold) in the absence of hormones on collagen fibrous substrates, but not on polycaprolactone fibrous substrates of equivalent orientation. ER inhibitors did not suppress cell proliferation on collagen fibrous substrates. The examination of reporter cells for ER signaling showed a lack of activity, thus confirming a shift toward an ER-independent proliferation mechanism. Examination of two selective inhibitors of $\alpha 2\beta 1$ and $\alpha 1\beta 1$ integrins showed that cell proliferation is suppressed in the presence of the $\alpha 2\beta 1$ integrin inhibitor only, thereby indicating that the observed changes in tumor cell behavior are caused by a combination of integrin signaling and/or an intrinsic structural motif that is uniquely present in the collagen fibrils. Adjacent coculture studies on collagen substrates showed that tumor cells on collagen can stimulate the proliferation of cells on tissue culture plastic through soluble factors. The magnitude of this effect correlated with the increased surface anisotropy of the substrate. This sensing in fibril orientation was further supported by a differential expression pattern of secreted proteins that were identified on random and aligned orientation substrates. Overall, this study shows a new role for electrospun collagen I fibrous substrates by supporting a shift toward an ER-independent tumor cell proliferation mechanism in ER+ breast tumor cells.


## Graphical Abstract

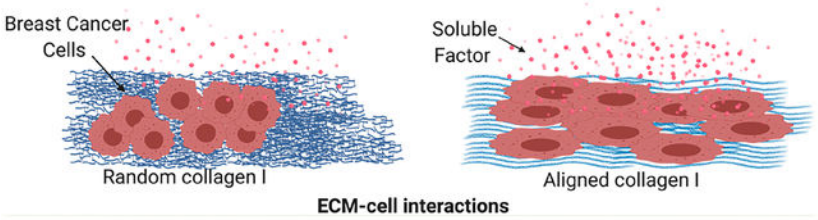



### Keywords

type I collagen; fibrous substrates; breast cancer cells; estrogen


## 1. INTRODUCTION

The physical properties of the fibrous collagen matrix are an ongoing interest topic to researchers. These have been linked to the progression of tumor cells toward a more aggressive phenotype and a poor prognosis in patients that are diagnosed with breast

cancer.[1,2] Type I collagen is one of the most abundant and studied components of the extracellular matrix (ECM), since its physical properties have been shown to play an essential role in tumor cell proliferation, migration, metastasis, and drug response.[3–5] Physical properties such as stiffness, topography, and organization significantly influence tumor cell behavior.[6] However, these properties have not been fully examined in culture models due to limitations in achieving independent control over the physical properties of the matrix during fabrication. Identifying such contributions is important for the generation and implementation of culture substrates supporting advanced tumor cell states. Matrix properties that challenge the outcome of therapy assays will pave a way to identify more robust therapeutic approaches.

The stiffness of the type I collagen matrix is one of the most studied physical parameters of the ECM and it is known to be a clinical prognosis marker of progression in breast tumors. High stiffness and density levels of the fibrous collagen matrix often correlate with fibril orientation and have been shown to promote tumor progression, invasion, and metastasis.[7–9] Keely and collaborators examined the implications of the collagen I matrix organization, density, and composition in breast tumor formation and progression. Three tumor-associated collagen signatures (TACS) that correlate with an invasive status were defined for tissue diagnosis. The examination of tissue specimens from 207 breast cancer patients showed that collagen alignment could be used as a physical parameter for tumor diagnosis.[10] Furthermore, tumor explant samples cultured in type I collagen showed matrix reorganization from a random orientation to an aligned orientation, facilitating cell migration and invasion.[8] Indeed, these observations have been recapitulated to some extent *in vitro* using collagen as a single matrix substrate. Recent investigations have shown that breast tumor cell migration is increased on anisotropic scaffolds when compared with isotropic collagen substrates.[11] Similarly, other studies show enhanced tumor cell invasion driven by the matrix orientation (aligned or random) and highlighted collagen fibril orientation as a more relevant parameter over stiffness in the observed tumor behavior.[11,12]

In addition to stimulating tumor cell invasion, the fibril structure and orientation of the type I collagen matrix may influence cell proliferation and drug sensitivity. For this reason, the examination of tumor cell–collagen matrix interactions in a growth-restrictive environment is an expanding topic of interest. Growth-restrictive environments such as those generated during hormone ablation therapy are of clinical interest since up to 30% of positive estrogen receptor (ER+) breast tumors will acquire resistance to the endocrine treatment's growth inhibitory effect.[13,14] Few cell-based studies have examined the impact of fibrous collagen I substrates as potential contributors to drug resistance in hormone-responsive breast tumors.[3] Examination of low- and high-density collagen substrates showed that matrix density plays an important role in the sensitivity of MCF-7 and T-47D breast cancer cells to 4-hydroxytamoxifen hormone ablation therapy.[15] Also, substrates with a stiffness of 0.4 kPa were found to promote the progression of ER (+) tumor cell lines as a consequence of estrogen cross-talk with prolactin.[15] Furthermore, modulation of drug sensitivity has also been reported on ER(−) tumor cells cultured on noncollagen-based fibrous scaffolds. Studies using 3D silk fibroin scaffolds showed that more than 6 times the usual concentration of the drug (doxorubicin) was needed to successfully inhibit the survival of the breast cancer

cell line MDA–MB–231 in these substrates.[16,17] Thus, these studies suggest that the fibrous matrix architecture or tumor cell microenvironment modulates the response to drug therapy.

Besides matrix stiffness, other physical properties, such as fibrous architecture, dimensionality, and orientation, may impact the proliferation and pharmacological response of ER(+) tumor cells, and yet this has not been clearly examined. Previous studies did not control the fibril orientation or diameter of the collagen matrix, without impacting substrate stiffness. Most cell-based studies employed self-polymerizing collagen I gels, a process that limits robust control over fibril diameter, orientation, and density on the micro- and nanoscales.[18] To enable examination of physical properties in a more independent manner, substrates generated by 3D printing or electrospinning methods are preferred since they enable fine-tuning over the fibrous substrates' physical properties. Our research group has previously reported a set of process parameters that enabled the generation of electrospun type I collagen fibrous scaffolds of controlled alignment (30–100%), without significantly impacting the diameter, density, and stiffness of the substrate.[5,19] Such fine control over processing parameters enables the gradual and consistent modification of physical properties for the independent measurements of the contributions of each physical property.

In this study, the surface orientation of electrospun type I collagen fibrils was manipulated independently of stiffness and fibril diameter to examine the effect of the fibrous structure and orientation in the proliferation and drug response of ER (+) breast tumor cells cultured in a hormone-restrictive environment.

## 2. MATERIALS AND METHODS

### 2.1. Cell Culture.

MCF-7 and T-47D, two human ER (+) breast carcinoma cell lines were used for this study. Both cell lines were purchased from American Type Culture Collection (ATCC). MCF-7 cells were maintained in DMEM high glucose media with L-Glutamine (D5796, Sigma-Aldrich) supplemented with 10% heat-inactivated fetal bovine serum (FBS; F6765, Sigma-Aldrich) and 1% penicillin/streptomycin (P4333, Sigma-Aldrich). T-47D cells were maintained in RPMI medium 1640 with L-Glutamine (11875–093, ThermoFisher Scientific) supplemented with 10% heat-inactivated FBS and 1% penicillin/streptomycin. RPMI and DMEM high glucose media without L-Glutamine, sodium pyruvate and phenol red (D1145, Sigma-Aldrich) supplemented with 10% FBS charcoal-stripped (F6765, Sigma-Aldrich) and 1% penicillin/streptomycin (P4333, Sigma-Aldrich) were used for the experimental conditions of MCF-7 and T-47D cells. All cells were cultured at 37 °C in a 5% $CO_2$ humidified environment. Cultures were periodically verified and confirmed to be free of mycoplasma. Passages were performed at 75–80% confluence using 0.5% trypsin (59418C, Sigma-Aldrich). Cell lines were used below 20 passages. Viable cells were identified using the Trypan Blue (T8154, Sigma-Aldrich) exclusion method and counted using a hemocytometer.

### 2.2. Fabrication of Electrospun Type I Collagen Substrates.

The collagen I used in this project was obtained from a bovine deep flexor tendon from Integra LifeScience. This type I collagen is of a high purity, and it has been used in many biomedical applications.[20] A collagen I solution was prepared by dissolving precut collagen I sponges (donated by Integra Lifesciences Holdings Corporations, Añasco, PR), in 90% v/v acetic acid (695092, Sigma-Aldrich) and distilled water to attain a final concentration of 20% w/v. This mixture was heated at 37 °C and magnetically stirred at 300 rpm on a hot plate for 72 h to ensure a constant range of kinematic viscosity (201–384 $mm^2/s$) across the different batches. The methodology for electrospun fibrils has been previously described in detail by Castilla-Casadiego et al.[21] Briefly, the electrospinning equipment used was custom built in our facilities and is composed of a power supply, an injection pump, a rotation drum, a Luer–Lock syringe, and a capillary steel needle of 1.5-in. length. The collagen solution was loaded into a 6 mL plastic syringe connected to a capillary blunt steel needle. The syringe was placed 20 cm from the rotating and oscillating drum collector that was covered with aluminum foil. An injection pump was used to push the solution from the syringe with a controlled flow rate of 3 mL/h. A power supply was used to induce 47 kV, with the positive pole connected to the steel needle and the negative pole connected to the collector.[5] The velocity of the drum collector determined the orientation of the fibrils, 3000 rpm for random collagen fibrils (RCF) and 15 000 rpm for aligned collagen fibrils (ACF). The relative humidity was kept in the 40–50% range during the electrospinning process. Collagen fibrils were cross-linked using glutaraldehyde (GA) vapor by using a volume of 30 mL of a 25% v/v GA solution (G6257, Sigma-Aldrich) in distilled water.[5] Humidity levels were kept under 60% during the cross-linking process that lasted approximately 24 h.

### 2.3. Physical and Chemical Characterization of Electrospun Collagen I Substrate.

Proton nuclear magnetic resonance ($^1$H NMR) characterization was performed on three batches of collagen I sponges to verify the biochemical composition across them. A multinuclear 500 MHz Bruker NMR equipped with QXI and BBO probes and four frequency channels was used to confirm chemical composition. All spectra were analyzed using Spinworks 4.2.10 software. To confirm that the biochemical composition of collagen was retained after the cross-linking process, Fourier transform infrared (FTIR) analysis was used to identify the vibrational bands of different functional groups that were present in the samples. Spectra were collected with a Spectrum Two FT–IR spectrometer by PerkinElmer with a wavenumber range of 500–4000 using 400 scans at 1 $cm^{-1}$ resolution.

The structural properties of electrospun collagen I and polycaprolactone (PCL) substrates were examined using spectroscopy and microscopy techniques. PCL substrates were purchased with defined fiber orientation [aligned (Z694614-12A; A-PCL) and random (Z694517-12EA; R-PCL)] from Sigma-Aldrich. Nevertheless, the level of orientation was verified for each substrate before culture studies. A VK-1X-000 Keyence microscope was used to determine the fibrils' degree of orientation based on the surface topography value of the Str (texture direction of the surface). Str can vary from 0 to 1, where values closer to 1 represent isotropic surfaces whereas values closer to 0 represent anisotropic surfaces. Specifically, values under 0.25 were considered as aligned orientation. AFM (Agilent model 5500, Keysight Technologies) was used to quantify the stiffness value of each substrate.

Contact mode scanning was conducted using a cantilever (Arrow-cont, NanoAndMore) reference of a force constant of 0.2 N/m, a resonance frequency of 14 kHz, and a length of 45 nm. Topographical analysis for stiffness measurements was carried out at room temperature. Areas with a scan size of 40 × 40 $\mu$m and scanning speed of 1.96 line/s were determined at 3–10 spots for each sample. Deflection sensitivity of 83.927 nm/V and five sweeps per point were used on the Picoview Software to analyze mechanical properties such as stiffness.

### 2.4. Culture Plate Setup of Cross-Linked Electrospun Collagen I Substrates.

The integration of electrospun fibrous substrates into microscale devices has been previously described in detail by Stallcop et al.[21] Briefly, cross-linked collagen membranes were bound to a double-sided medical grade tape (ARCare 90106) and cut out as circles of diameters between 6 mm and 22 mm (depending on the well plate to be used). A cutting plotter (CE5000–40-CRP, Graphtec America, Irvine, CA, USA) equipped with a 0.9 mm diameter and 60° angle Graphtec blade (CB09UA) was used to generate the circles. This collagen-tape laminate was then taped down to the bottom of culture plates or in the culture regions of the open-well culture device.[21] Culture surfaces were sterilized prior to cell seeding. The sterilization process consisted of three sequential washes with PBS 1×, followed by two cycles of 15 min exposition to UV light. The cell culture medium was incubated overnight to confirm sterility before cell seeding.[5]

### 2.5. Preparation of Gelatin and Collagen I Gel Substrates.

For gelatin-coating substrate (gelatin), a volume of 50 $\mu$L of gelatin (6950, Cell biologics) solution was added to the wells of a 96-well plate for 15 min. The excess solution was removed before seeding cells at room temperature inside a biosafety cabinet. For collagen gel (gel), a high concentration rat tail collagen (354249, Corning Life Sciences) was neutralized with 1N NaOH (S318, Fisher Scientific) and 10× PBS (59331C, Sigma-Aldrich) and then mixed with media containing the desired cell density until a final collagen concentration of 3 mg/mL. The final solution was incubated at 37 °C for 15–20 min and then hydrated with phenol-free culture media.[22]

### 2.6. Hormone-Free Cultures and Pharmacological Inhibition of ER.

Tumor cell studies were carried out in hormone-free culture conditions to maintain basal cell proliferation levels below 10% in estrogen-dependent cell lines, for both MCF-7 and T-47D. Cells cultured in T25 flasks were washed twice with 3 mL of PBS 1× followed by incubation in 5 mL of phenol-free DMEM (D1145, Sigma-Aldrich) supplemented with 1% penicillin–streptomycin and 10% charcoal-stripped FBS (F6765, Sigma-Aldrich) for 72 h. Cells were detached with a phenol-free 1× trypsin (59418C, Sigma-Aldrich), and viable cells were counted with a hemocytometer using the trypan blue (T8154, Sigma-Aldrich) exclusion method. Approximately 100,000 cells/cm$^2$ were seeded in 96-well plates and incubated at 37 °C and 5% $CO_2$. The culture medium was replaced after 24 h with phenol-free DMEM that was supplemented with 1% penicillin–streptomycin and 10% charcoal-stripped FBS ± 1 nM estrogen (E2758, Sigma-Aldrich) and Fulvestrant (S1191, Selleckchem) or Tamoxifen (S1972, Selleckchem), both at a concentration of 10 nM.[23] Tissue culture plastic (TCP) was used as the standard substrate control for proliferation

and response to ER inhibitors. After an incubation period of 72 h, cell proliferation was examined. The conditions that displayed significant cell proliferation changes were used to evaluate integrin and soluble factor mechanisms, gene expression, and secreted soluble factor profile in the microwell culture platform.

### 2.7. Proliferation Assay.

Tumor cell proliferation was monitored using the Click-iT Plus EDU Alexa Fluor 488 Flow Cytometry Assay Kit (C10420, Thermo Fisher Scientific) and Click-iT Plus EDU Alexa Fluor 488 Imaging Assay Kit (C10337, Thermo Fisher Scientific) following the manufacturer's recommendations. Proliferation measurements were obtained using a BD Accuri C6 flow cytometry while a VK-1X-000 Keyence microscope was used for the imaging sample.

### 2.8. Cell Nuclear Shape.

A nuclear shape factor was used to characterize nuclear elongation with the relation between the minor and major axis of the nucleus.[24] Cell nuclei were stained with hoechst 33342 (1:1000, H3570, ThermoFisher Scientific). Prior to staining with hoechst, cells were fixed with 4% paraformaldehyde (50–980–487, Fisher Scientific) for 20–30 min and washed three times with PBS 1×. Images taken with fluorescent microscopy were analyzed to obtain the value of the nucleus axis (major axis and minor axis), using ImageJ software. At least 20 nuclei were analyzed per image. Nuclear elongation values closer to 1 correspond to more rounded nuclei, whereas values closer to 0 correspond to more elongated nuclei.

### 2.9. $\alpha_2\beta_1$ Integrin Inhibition.

To evaluate the integrin signaling mechanism, the proliferation of MCF-7 cells was evaluated in hormone-depleted media with a treatment that consisted of two integrin inhibitors: $\alpha_2\beta_1$, 132 nM BTT 3033 (4724, Tocris), and $\alpha_1\beta_1$, Obtustatin 0.8 nM (4664, Tocris). The cell seeding procedure was the same as described in section 2.6. Culture media were replaced with fresh phenol-free DMEM (supplemented with 1% penicillin–streptomycin and 10% charcoal-stripped FBS ± BTT 3033 or Obtustatin) 24 h after cell seeding. After an incubation period of 72 h, cell proliferation was examined as described in section 2.7.

### 2.10. Western Blot.

Cells were lysed using RIPA buffer (R0278, Sigma-Aldrich) with a 10% protease inhibitor (K271–500, BioVision) to yield whole-cell extracts. Protein concentration was determined using a BCA Assay kit (23225, ThermoFisher) following the manufacturer's instructions and was measured on a Spark Multimode plate reader (Tecan). Samples were resolved in a Bolt 4 to 12%, Bis-Tris, 1.0 mm, Mini Protein gel (NW04120BOX, Invitrogen) using a mini gel tank (A25977, Invitrogen). Proteins were transferred to a nitrocellulose membrane with iBlot 2 Transfer Stacks (IB23002, Invitrogen) in an iBlot 2 Gel Transfer Device (IB21001, Invitrogen). Membranes were blocked using a blocking solution composed of 5% dry milk, 0.02% sodium azide (S2002, Sigma-Aldrich), and 0.2% Tween 20 in PBS 1× (PBST; P9416, Sigma-Aldrich). Membranes were then incubated in the same blocking

solution containing primary antibodies for anti-FAK (phospho; ab81298, Abcam), anti-FAK (ab76496, Abcam), anti-ERK (phospho; ab223500, Abcam), anti-ERK (ab17942, Abcam) or $\beta$-actin (ab8226, Abcam). After overnight incubation, blots were washed with a PBST solution before incubation with secondary antibodies conjugated to horseradish peroxidase (ab6789 and ab6721, Abcam) diluted in blocking solution without sodium azide for 1 h. Expression levels of $\beta$-actin were used as a loading control to ensure an equivalent loading of samples. Protein bands were visualized by enhanced chemiluminescence (sc-2048, Santa Cruz Biotechnology) in a ChemiDoc XRD System (Bio-Rad). Band intensities were quantified using Image Lab Software, Bio-Rad.

### 2.11. Secretome Analysis.

Conditioned media (2 mL/sample) were collected from tumor cells that were seeded at 100,000 cells/cm$^2$ and cultured for 2 days. Collected media were centrifuged at 250 rcf for 5 min, and the supernatant was collected and stored at −80 °C. Frozen samples were sent to RayBiotech for quantitative proteomic analysis using the 640 Human protein arrays (QAH-CAA-640–1, RayBiotech). Data were compared across culture substrates to identify significant changes in secreted factors. First, protein data in picograms per milliliter were adjusted by media volume and number of cells. These adjusted measurements were used to calculate fold changes (FC) for culture substrates, random and aligned relative to TCP protein concentrations. Differentially expressed proteins (DEPs) were defined as proteins with FC values that were above 4 or less than 0.25. Proteins with expression values equal to zero (i.e., low detection limit) were discarded from this analysis. The Venn Diagram package in R was used to generate the logical relationship diagram.[25]

### 2.12. Statistical Analysis.

Two-way ANOVA with Tukey's multiple comparisons analysis was used to compare changes with respect to baseline values or treatment controls. The significance level ($\alpha$) was set to ≤0.05, except for the normality diagnostic test ($p > 0.05$). IBM SPSS (Chicago, IL), v.23.0 for Windows and GraphPad Prism 7 (GraphPad Software, CA, USA) were used. Wilcoxon–Mann–Whitney test was performed when the data failed to follow a normal distribution. *P* values below 0.05 were considered significant as follows: *$p < 0.05$, **$p < 0.01$, ***$p < 0.001$, and ****$p < 0.0001$.

## 3. RESULTS

### 3.1. Synthesis and Characterization of Collagen Fibrils.

Collagen fibrils were generated by the electrospinning method followed by cross-linking with glutaraldehyde to maintain their structural stability in an aqueous solution. The biochemical composition of collagen I was examined in three independent batches using $^1$H NMR to discard collagen purity variations and discard its further impact on cell behavior. The main structure of collagen results from the abundance of three primary amino acids with the repeating motif Gly–X–Y, where X and Y positions are often proline and hydroxyproline or any amino acid.[26–28] Some chemical shifts of these amino acids are shown in the $^1$H NMR spectrum, representing some interactions between neighboring hydrogens and confirming the presence of main components in the collagen I source used. Figure 1A shows

$^{1}$H NMR spectra of three batches of collagen I examined presenting the same resonance and intensities that are attributed to the proton of amide bond $a$ = 8.6,[29] CH group $b$ = 4.68 (hydroxyproline),[30] $c$ = 3.65 (proline and glycine),[31] $d$ = 3.28 (Proline),[31] and $CH_2$ group $e$ = 2.07 (proline and hydroxyproline).[31,32] Therefore, these data confirm that the molecular weight and purity of collagen I remain constant through the different batches used experimentally.

FTIR spectroscopy indicates that the collagen I membranes retained their functional groups, confirming that the biochemical structure of collagen I was not affected after the cross-linking process. Figure 1B shows a representative spectrum of collagen fibrils for three fibril batches of cross-linked and un-cross-linked collagen. Bands around 1630 $cm^{-1}$ correspond to strong C=O stretching of amide I in peptides;[33,34] the weak peak at 1480–1575 $cm^{-1}$ is attributed to the N–H bending of amide II and the moderate band at 1229–1301 $cm^{-1}$ by the bending of N–H and CN stretching for amide III.[35,36] The band around 3300 $cm^{-1}$ is attributed to amide A, a specific band for proteins,[5] and the band at 3080 $cm^{-1}$ to the spectral feature of the amide B that arises from C–H stretching. The positions on these amide bands did not shift in both samples, indicating that the functional groups were maintained after cross-linking as previously reported in our studies.[5]

To determine the degree of anisotropy of the substrates, the surface properties of the electrospun substrates were examined. Representative images are shown in Figure 1C with an inset of the angle spectrum that measures the direction of the fiber's angles. Commercially available PCL substrates were used as reference controls for aligned and random orientations. TCP and gelatin were used as reference controls for isotropic surfaces. Surface images of all substrates are shown in Figure S1. The uniformity of the texture surface (Str ratio) was used to discriminate between random, aligned, and isotropic surfaces. Table 1 shows the average Str value for the different substrates, ranging from 0.06 to 0.7. It is important to define that values under 0.25 were considered to represent uniform orientation (aligned), values >0.28 and <0.50 were considered of random orientation, and values >0.50 were considered isotropic (undefined orientation).[37,38] For these studies, TCP, gelatin-coated TCP, and collagen gel were grouped as isotropic substrates and collagen and PCL fibrous substrates were grouped as anisotropic substrates.

Stiffness often depends on the degree of polymerization (solid status) and structure of the substrate. Hence, semisolid substrates (e.g., gels) will have a lower stiffness than more solid or fibrous architectures. To determine each culture substrate's stiffness, AFM images were analyzed using Pickofview software (see Figure S1 for AFM Images). Table 1 shows the young modulus values computed for each substrate. As expected, TCP and gelatin coating had the highest substrate stiffness with values on the order of $10^6$, which is comparable to those reported in the literature.[39] Collagen gel had the lowest stiffness value.[40] Fibrous collagen and PCL[29,41] stiffness values were very similar and fell within the physiological range of values reported for human tissue.[42,43] The stiffness and diameter values obtained for electrospun collagen I are within the range of those reported in breast tissues (0.5–15 kPa and 0.5–3.5 $\mu$m).[44,45]

### 3.2. Effects of Collagen Substrates on Tumor Proliferation in a Hormone-Restricted Microenvironment.

The proliferation of MCF-7 and T-47D cells was evaluated under hormone-restrictive culture conditions using both electrospun and standard culture substrates. TCP and gelatin-coated TCP were used as a 2D standard substrate and collagen I gel as a 3D for undefined orientation. Commercial electrospun PCL substrates characterized in Table 1 were used as a positive control for fibrils orientation. Cells were cultured on each substrate for 72 h. Estrogen was used as a positive control for cell proliferation and was added during the last 48 h of culture. Cells in the S phase were labeled with EdU during the last 2 h of culture. As expected, preconditioning the estrogen-dependent breast tumor cells to a hormone-depleted environment limited the proportion of cells in the S phase to levels below 15–20% (vehicle). Reduced proliferation was observed for both cell lines in the absence of estrogen when cultured on TCP, gelatin-coated TCP, collagen I gel, and PCL fibrils (Figure 2A,B). As expected, cell proliferation was enhanced in the presence of an estrogen ligand (E2). However, cells in the vehicle group that were cultured on electrospun collagen fibrous substrates showed a significant increase in cell proliferation on both random and aligned fibril orientations. This enhanced cell proliferation level was equivalent to or higher than those observed in the estrogen-treated TCP group. To determine whether the fibril diameter had an impact on the observed cell behavior, cell proliferation was compared among collagen substrates of approximately 1 and 0.3 $\mu$m fibril diameter (see Figure S2). Results showed no significant difference in cell proliferation indicating that an increment of 3× in fibril diameter does not affect the observed cell response. For cellular studies, collagen fibrous substrates of an average fibril diameter of 0.3 $\mu$m were selected due to their reduced background noise during fluorescent image acquisition.

To confirm that ER signaling was suppressed and had not been activated through an estrogen-independent mechanism, the same culture conditions were examined using a luciferase reporter MCF-7 cell line. The MCF-7 MVLN cell line stably expresses an estrogen responsive element promoter–luciferase reporter gene construct that is activated in response to ER signaling. Consequently, results shown in Figure S3 show a 3-fold increase in luminescence only in the presence of estradiol but not in the vehicle or collagen substrate conditions, indicating that the proliferation mechanism observed on collagen I fibrils is independent of ER signaling.

Since differences in cell proliferation were not detected between aligned and random fibers, cell elongation was examined as an indicator of physical changes perceived at the cell level. Cell elongation is an indicator of the nuclear and cytoskeletal organization on anisotropic substrates. The nuclear shape factor was quantified to identify a potential correlation between cell proliferation and elongation. The nucleus elongation was obtained as a ratio of the minor (green line on the zoom image of Figure 2C) and major (red line on the zoom image of Figure 2C) axes of the nucleus (additional representative images are shown in Figure S4). A nuclear shape factor with a value of 1 corresponds to a perfectly round nucleus and a nuclear shape factor close to 0 corresponds to a more elongated shape. As expected, results indicate that cells on ACF and A-PCL are more elongated (Figure 2D) than in random and isotropic substrates confirming a positive impact of fibril alignment

on cell elongation as reported before for cell invasive phenotypes.[46] However, because cell elongation is a parameter associated with enhanced cell invasion, this parameter was not indicative of the observed changes in cell proliferation.[46] Thereby, the observed enhanced cell proliferation on collagen I is likely associated with biochemical signaling and not a mechanical stimulus driven by the fibrous matrix.

### 3.3. Effect of Collagen Fibrous Substrates in Response to Endocrine Therapy.

In addition to controlling hormone availability, pharmacological inhibitors of the ER are broadly used as the main line of therapy to suppress hormone signaling in ER+ breast tumors.[47,48] Tamoxifen (TAM) and Fulvestrant (FULV) are two clinical pharmacological ER inhibitors that target ER to inhibit estrogen-dependent tumor growth, working as an agonist and antagonist, respectively.[49,50] Here, TAM and FULV were used to examine the influence of fibrous structure and orientation of collagen I substrates in the growth inhibitory effect of ER inhibitors. Figure 3 summarizes the proliferation values of MCF-7 cells relative to the vehicle condition on TCP. In the absence of estrogen, a marked effect on cell proliferation was not observed in TCP, gelatin, collagen I gel, R-PCL, or A-PCL substrates (Figure 3A–C,F,G) after treatment with both TAM and FULV. As expected, in the presence of estrogen, an inhibitory effect on cell proliferation was observed for both drugs, reaching levels equivalent to the vehicle condition on TCP. However, the growth inhibitory activity of both drugs was suppressed for cells cultured on collagen I fibrous substrates independently of the fibril orientation (Figure 3D,E). These data suggest that the fibrous collagen I matrix decreased drug sensitivity or enabled a shift in the proliferation mechanism, or both.

It has been reported that the ECM can increase chemotherapy resistance by preventing the penetration of drugs in the cancer cells. This occurs through interactions between the cancer cells and ECM components that can affect the apoptosis resistance.[51,52] To determine whether the observed reduced drug sensitivity was associated with a limited drug diffusion in the matrix, the concentration of Tamoxifen was increased by 100-fold relative to the E2 concentration (1 nM). Results shown in Figure 3H indicate a marked reduction in the proliferation of cells on TCP substrates only. The proliferation behavior persisted on fibrous collagen substrates treated with estrogen + tamoxifen, independently of the fibrils' orientation. This decrease in sensitivity of ER inhibitors was also observed in the T-47D cell line (Figure S5). The data suggest a shift toward an estrogen-independent proliferation mechanism in which the type I collagen matrix stimulates the proliferation of tumor cells in the absence of hormones and the presence of ER inhibitors.[53]

### 3.4. Inhibition of Collagen I Binding Integrins.

Integrins are the major group of receptors for cell adhesion to the ECM. Interactions regulated by integrin-ECM mechanisms have been shown to trigger many intracellular pathways to stimulate cell growth and prevent entry into the cell death cycle.[54–56] Collagen I is the main component of the ECM, and several cell integrins contain collagen I–binding domains.[57] Thus, we hypothesized that the observed proliferation stimulation in the absence of hormones was associated with an integrin–matrix interaction rather than the fibril orientation of the collagen I substrates. To test this hypothesis, first cell proliferation was examined on nonintegrin binding PCL fibrous substrates. MCF-7 cells were cultured on PCL

substrates of random and aligned orientation for 72 h ± exogenous addition of estrogen. Results show no significant effects on the proliferation of cells in the absence of estrogen stimulation (Figure 4A), and as expected, exogenous estrogen (E2) significantly enhanced cell proliferation across all substrates. The effect of estrogen on cell proliferation was incremental as follows: aligned PCL > random PCL > TCP. These results indicate that fibril orientation can stimulate cell proliferation in the presence of estrogen. However, cell-matrix signals, such as integrins, are needed for proliferation stimulation in the absence of estrogen.

To examine the impact of integrin activity on the observed increase of cell proliferation in the absence of estrogen, the activity of $\alpha_1\beta_1$ and $\alpha_2\beta_1$, two major integrins that bind to collagen I, were targeted with pharmacological inhibitors. BTT 3033 and Obtustatin are selective inhibitors for integrins $\alpha_2\beta_1$ and $\alpha_1\beta_1$, respectively. The drug concentrations used were determined based on the preliminary assessment of cell viability in TCP using reported IC50 values.[58] Gelatin-coated TCP and type I collagen gel were used as nonfibrous positive controls for $\alpha_1\beta_1$ and $\alpha_2\beta_1$ activity, respectively. As expected, both drugs had no significant inhibitory effect on cell proliferation (Figure 4B,C). Examination of the proliferation of MCF-7 cells on collagen fibrous substrates showed a significant reduction in groups treated with BTT 3033-a (Figure 4D,E). Obtustatin had no significant inhibitory effects in MCF-7 cells that were cultured on collagen I fibrous substrates (Figure 4F,G). Thus, the data suggest that $\alpha_2\beta_1$ integrin signaling is involved in regulating cell proliferation in the absence of estrogen on electrospun collagen I substrates.

Integrin downstream signaling depends on the activation of focal adhesion kinase (FAK) and extracellular-signal-regulated kinase (ERK). This activity has been the main interest as a therapeutic alternative for some cancers.[59–61] To confirm that the used integrin inhibitors were targeting integrin downstream signaling, activity levels of FAK and ERK were examined in MCF-7 cells that were cultured in TCP and collagen fibrous substrates in a hormone-restricted culture. As expected, Figure 5 shows that the ratio of phosphorylated FAK to total FAK is increased by approximately 3 fold on collagen substrates as compared to TCP. Ratios of phosphorylated ERK to total ERK were not affected across the substrates. Treatment with BTT 3033 or Obtustatin significantly reduced ERK and FAK ratios in both aligned and random collagen substrates but not in TCP, confirming targeting of this downstream signaling mechanism. Both inhibitors downregulate FAK signaling activity. However, FAK activity as a main downstream target of BTT that is associated with the observed inhibition of cell proliferation on collagen fibrils cannot be rule out. Therefore, it is likely that other signals are involved in supporting cell proliferation downstream of $\alpha_2\beta_1$ integrin activity.

### 3.5. Soluble Factor-Mediated Effect and Secretome Profile.

To determine whether the stimulation of cell proliferation on collagen fibrils required direct cell contact with the collagen fibrils, tumor cells on TCP were examined after coculture with cells on collagen substrates using a 2-microwell nested array (Figure 6A). MCF-7 cells that were seeded on TCP were cultured adjacent to MCF-7 cells that had been seeded on TCP (vehicle), gelatin, RCF, or ACF substrates. Exogenous addition of estrogen (E2) was used as a positive control for cell proliferation. Examination of cultures at 72 h

showed stimulation of cell proliferation in TCP (Figure 6B). The proliferation of cells on TCP was incremental in the following order: gelatin < RCF < ACF. Cells on aligned substrates (ACF) were more potent than random substrates (RCF), which suggests that cells sensed changes in fibril orientation, consequently modifying their secretome. To identify differences across substrates at the secretome level, conditioned media were examined for 640 human factors in both MCF-7 and T47D (Table S1). The number of factors with changes of ±4 fold with respect to TCP are shown in Figure 6C. Even though differentially secreted factors were not found in common across all conditions, totals of 67 and 19 factors were differentially expressed in fibrous substrates relative to TCP in MCF-7 and T47D, respectively. Moreover, three secreted factors (EDAR, PDGF-CC, TFPI) showed distinct secretion profiles that were relative to TCP within the culture substrate of aligned orientation regardless of the cell type. Both cell secretomes showed significant downregulation of PDGF-CC and TFPI. Nonetheless, EDAR was highly secreted in T47D cells with aligned culture substrates compared with TCP, while the opposite secretion pattern was observed in MCF-7. Furthermore, 11 factors (Glypican 5, Calcitonin, Endocan, GDF-8, Insulin R, BAMBI, Carbonic Anhydrase XII, GPR56, RBP4, Dkk-4, and OPG) were commonly identified as differentially secreted factors among culture substrates with random orientation relative to TCP in both MCF-7 and T47D. These secreted factors showed lower levels in culture substrates of random orientation than in TCP except for RBP4 and Dkk-4 factors with fold changes of 4.02 and 5.25, respectively.

## 4. DISCUSSION

Cell culture experiments conducted with tumor cells indicate that fibrils of type I collagen appear to be sufficient to promote cell proliferation in the absence of hormones and to decrease sensitivity to ER inhibitors. The same result was not observed in gelatin, collagen gel, and PCL fibrous substrates, suggesting that this unexpected result may be caused by a combination of integrin signaling and an intrinsic structural motif uniquely present in the collagen fibrils. Both the electrospun collagen and the fibrils resulting from the spontaneous exothermic polymerization in a collagen gel can exhibit a banding pattern. However, gel’s stiffness is lower and lacks structural uniformity when compared to the electrospun substrate. It is therefore clear that these two types of collagen substrates have subtle structural differences that are perceived at the cellular level.

The data shown here indicate that the electrospun collagen I substrate supports a shift in the cell proliferation mechanism from ER-dependent to ER-independent, thereby decreasing the sensitivity of breast tumor cells to standard pharmacological ER therapy. Moreover, the culture of the cells on collagen fibrous substrates was sufficient enough to stimulate the proliferation of adjacent cells on TCP through secreted factors. This implies that direct contact with the matrix is not required to significantly impact the proliferation of surrounding cells or the bulk tumor population at the tissue level. To our knowledge, this is the first report that sheds lights on such a collagen matrix-driven proliferation mechanism which likely influences tumor cell survival during ER therapy at an early stage before achieving an invasive tumor cell phenotype. Such findings are of clinical relevance because identifying such ER-independent proliferation mechanisms may lead the development of a

combinatorial therapy approach that might prevent these cells from surviving and becoming invasive.

Although a significant change in cell proliferation due to the orientation of the fibrils of the collagen I substrate was not captured, a differential potency effect and expression pattern of soluble secreted factors were detected, indicating that cells sense changes in fibril orientation, which can impact the bulk tumor population. This might explain the reported correlation of matrix alignment with the progression of breast tumors, even though the distribution of such matrix patterns is not uniform across the tumor tissue.[10] One potential target to disrupt such interaction is the $\alpha_2\beta_1$ integrin, whose signaling activity is associated with the fibril structure of the collagen I substrate. This highlights the importance of the fibril condition in modulating tumor progression. However, targeting integrins are a difficult therapeutic strategy to deliver systemically due to their ubiquitous expression and activity in tissues. Thereby, the specific downstream mechanism still needs to be determined to examine other therapeutic approaches that are more targetable.

Several factors were downregulated in tumor cells that were cultured in fibrous substrates (Figure 6). From those, EDAR and TFPI have been shown to induce cell death in breast cancer,[62] while Glypican 5 and GDF8 have been linked to anchorage-independent growth of lung cancer cells[63,64] and malignant breast adenocarcinoma,[65] respectively. Thus, collectively, the collagen I fibrous matrix instructs a local microenvironment that is more antiapoptotic and supportive of a transition toward a more invasive cell phenotype. Whether a single factor or a combination of them are indeed implicated in the observed tumor behavior should be further investigated to determine their collective impact in the progression of breast tumors and identify new venues for therapy.

Given the importance of the fibrous structure of the collagen I matrix in supporting the oncogenic activity of tumor cells,[7,9] the integration of such fibrous substrates should be considered in drug potency assays. The progression toward advanced stages includes cell invasion and earlier steps such as hormone-independent growth of ER+ tumor cells and decreased drug sensitivity. Both steps are shown to be supported by the fibrous structure of the collagen I matrix. Standard drug potency assays use single-cell models on flat culture surfaces, which will not enable the identification of therapeutic compounds that are targeted to cell–matrix interactions. In turn, these interactions are associated with the progression of tumor cells toward advanced stages. A barrier for the integration of collagen I fibrous substrates in drug potency assays is the lack of control over the matrix architecture and its shelf stability, which increases the collected data’s variability across technical replicates and, also, the reproducibility of the experimental studies. Part of the limitation is that the self-polymerization of processes commonly used for collagen gelation often depend on the incubation time and environmental conditions. As such, an increase in substrate stiffness is the result of an increase in the solidification status of the matrix, due to the cross-linking level and maturity of the structures that were formed. Since this solidification often occurs in small volumes, when increases in temperature and humidity are not controlled, the resulting stiffness has some variability across replicates and experiments. This variability is caused by the microscopic structures of the matrix, which includes multiple fibril diameters in combination with less mature structures and a nonuniform distribution. This

forces the examination of cell behavior in single cells or small clusters aided through high magnification microscopy to establish a correlation with a particular matrix property. Moreover, once fabricated, these substrates have to be used immediately or they will have a short preservation time under refrigerated conditions. The lack of stability and uniformity of the collagen gel substrates can lead to heterogeneous tumor cell changes within the bulk population. This can mask clinically relevant cell phenotypes, thereby limiting its use into preclinical high-throughput preclinical assays such as drug screening and genomic profiling. A way to address this limitation is to employ electrospun substrates of defined structure and composition that can be easily incorporated into conventional well-based culture platforms. Fibrous substrates with defined physical parameters can be generated via electrospinning to achieve a more homogeneous structural arrangement and mimetic of the native ECM tissue. The electrospun collagen I substrates used in this study preserved their native structure for over 3 months and did not require refrigeration, providing easy handling and transportation. Importantly, our group has incorporated these defined ECM structures into a multiadjacent microwell platform with a user-friendly layout and interface for fast prototyping (<10 min) in conventional laboratory settings.[21] One drawback of the electrospinning approach is that it only provides a flat surface that is incompatible with spheroid cultures and other 3D culture methods, which are important for phenotypic cell models such as stem cells. Strategies, such as 3D printing methods, should be explored to fine-tune the fibril architecture in a volumetric fashion that could commence a potential study of fibrous substrates in 3D cultures.

## 5. CONCLUSION

Overall, the study shows that the collagen I fibrous matrix supports tumor cell proliferation in an ER-independent manner. This effect can be potentiated by changes in the orientation of the collagen I fibrils. Such changes in tumor cell behavior are driven by an intrinsic structural motif uniquely present in the collagen fibrils. Therefore, the integration of fibrous substrates into *in vitro* studies and drug assays is anticipated to lead the discovery of new therapeutic venues.

## Supplementary Material

Refer to Web version on PubMed Central for supplementary material.

## ACKNOWLEDGMENTS

We would like to thank Dr. David Suleiman and his Ph.D. student Karen Barrios Tarazona for their collaboration with the substrates' characterization using AFM, David A. Castilla-Casadiego for electrospinning training, and José Almodóvar for assisting with the acquisition of images using confocal microscopy. We also thank Adhesives Research, Inc. for generously donating the ARCare 90106 tape for micro-fabrication and Integra Lifesciences Holdings Corporations, Añasco, PR for donating the collagen I sponges used in this study. The authors declare no financial interest.

## REFERENCES

(1). Xiong G-F; Xu R Function of Cancer Cell-Derived Extracellular Matrix in Tumor Progression. Journal of Cancer Metastasis and Treatment 2016, 2, 357.

(2). Hynes RO The Extracellular Matrix: Not Just Pretty Fibrils. Science 2009, 326 (5957), 1216–1219. [PubMed: 19965464]

(3). Işeri OD; Kars MD; Arpaci F; Gündüz U Gene Expression Analysis of Drug-Resistant MCF-7 Cells: Implications for Relation to Extracellular Matrix Proteins. Cancer Chemother. Pharmacol 2010, 65 (3), 447–455. [PubMed: 19543729]

(4). Benton G; DeGray G; Kleinman HK; George J; Arnaoutova I In Vitro Microtumors Provide a Physiologically Predictive Tool for Breast Cancer Therapeutic Screening. PLoS One 2015, 10, e0123312. [PubMed: 25856378]

(5). Castilla-Casadiego DA; Ramos-Avilez HV; Herrera-Posada S; Calcagno B; Loyo L; Shipmon J; Acevedo A; Quintana A; Almodovar J Engineering of a Stable Collagen Nanofibrous Scaffold with Tunable Fiber Diameter, Alignment, and Mechanical Properties. Macromol. Mater. Eng 2016, 301, 1064–1075.

(6). Guzman A; Ziperstein MJ; Kaufman LJ The Effect of Fibrillar Matrix Architecture on Tumor Cell Invasion of Physically Challenging Environments. Biomaterials 2014, 35, 6954–6963. [PubMed: 24835043]

(7). Jena MK; Janjanam J Role of Extracellular Matrix in Breast Cancer Development: A Brief Update. F1000Research 2018, 7, 274. [PubMed: 29983921]

(8). Provenzano PP; Eliceiri KW; Campbell JM; Inman DR; White JG; Keely PJ Collagen Reorganization at the Tumor-Stromal Interface Facilitates Local Invasion. BMC Med. 2006, DOI: 10.1186/1741-7015-4-38.

(9). Provenzano PP; Inman DR; Eliceiri KW; Knittel JG; Yan L; Rueden CT; White JG; Keely PJ Collagen Density Promotes Mammary Tumor Initiation and Progression. BMC Med. 2008, 6, 11. [PubMed: 18442412]

(10). Conklin MW; Eickhoff JC; Riching KM; Pehlke CA; Eliceiri KW; Provenzano PP; Friedl A; Keely PJ Aligned Collagen Is a Prognostic Signature for Survival in Human Breast Carcinoma. Am. J. Pathol 2011, 178 (3), 1221–1232. [PubMed: 21356373]

(11). Campbell JJ; Husmann A; Hume RD; Watson CJ; Cameron RE Development of Three-Dimensional Collagen Scaffolds with Controlled Architecture for Cell Migration Studies Using Breast Cancer Cell Lines. Biomaterials 2017, 114, 34–43. [PubMed: 27838472]

(12). Riching KM; Cox BL; Salick MR; Pehlke C; Riching AS; Ponik SM; Bass BR; Crone WC; Jiang Y; Weaver AM; Eliceiri KW; Keely PJ 3D Collagen Alignment Limits Protrusions to Enhance Breast Cancer Cell Persistence. Biophys. J 2014, 107, 2546–2558. [PubMed: 25468334]

(13). Musgrove EA; Sutherland RL Biological Determinants of Endocrine Resistance in Breast Cancer. Nat. Rev. Cancer 2009, 9 (9), 631–643. [PubMed: 19701242]

(14). Schiff R; Massarweh S; Shou J; Osborne CK Breast Cancer Endocrine Resistance: How Growth Factor Signaling and Estrogen Receptor Coregulators Modulate Response. Clin. Cancer Res 2003, 9, 447S–54S. [PubMed: 12538499]

(15). Barcus CE; Holt EC; Keely PJ; Eliceiri KW; Schuler LA Dense Collagen-I Matrices Enhance Pro-Tumorigenic Estrogen-Prolactin Crosstalk in MCF-7 and T47D Breast Cancer Cells. PLoS One 2015, 10, e0116891. [PubMed: 25607819]

(16). Mandal BB; Kundu SC Cell Proliferation and Migration in Silk Fibroin 3D Scaffolds. Biomaterials 2009, 30, 2956–2965. [PubMed: 19249094]

(17). Talukdar S; Mandal M; Hutmacher DW; Russell PJ; Soekmadji C; Kundu SC Engineered Silk Fibroin Protein 3D Matrices for in Vitro Tumor Model. Biomaterials 2011, 32 (8), 2149–2159. [PubMed: 21167597]

(18). Truong D; Puleo J; Llave A; Mouneimne G; Kamm RD; Nikkhah M Breast Cancer Cell Invasion into a Three Dimensional Tumor-Stroma Microenvironment. Sci. Rep 2016, DOI: 10.1038/srep34094.

(19). Castilla-Casadiego DA; Maldonado M; Sundaram P; Almodovar J Green" Electrospinning of a Collagen/hydroxyapatite Composite Nanofibrous Scaffold. MRS Commun. 2016, 6, 402–407.

(20). Duragen-xs. https://www.integralife.com/duragen-xs/product/dural-repair-grafts-duragen-xs (accessed March 10, 2020).

(21). Stallcop LE;Álvarez-García YR; Reyes-Ramos AM; Ramos-Cruz KP; Morgan MM; Shi Y; Li L; Beebe DJ; Domenech M; Warrick JW Razor-Printed Sticker Microdevices for Cell-Based Applications. Lab Chip 2018, 18 (3), 451–462. [PubMed: 29318250]

(22). Barkal LJ; Procknow CL;Álvarez-García YR; Niu M; Jiménez-Torres JA; Brockman-Schneider RA; Gern JE; Denlinger LC; Theberge AB; Keller NP; Berthier E; Beebe DJ Microbial Volatile Communication in Human Organotypic Lung Models. Nat. Commun 2017, 8 (1), 1770. [PubMed: 29176665]

(23). Huynh H; Nickerson T; Pollak M; Yang X Regulation of Insulin-like Growth Factor I Receptor Expression by the Pure Antiestrogen ICI 182780. Clin. Cancer Res 1996, 2 (12), 2037–2042. [PubMed: 9816164]

(24). McGrail DJ; Ghosh D; Quach ND; Dawson MR Differential Mechanical Response of Mesenchymal Stem Cells and Fibroblasts to Tumor-Secreted Soluble Factors. PLoS One 2012, 7 (3), e33248. [PubMed: 22438903]

(25). Chen H; Boutros PC VennDiagram: A Package for the Generation of Highly-Customizable Venn and Euler Diagrams in R. BMC Bioinf. 2011, 12, 35.

(26). Brodsky B; Ramshaw JAM The Collagen Triple-Helix Structure. Matrix Biol. 1997, 15, 545–554. [PubMed: 9138287]

(27). Belbachir K; Noreen R; Gouspillou G; Petibois C Collagen Types Analysis and Differentiation by FTIR Spectroscopy. Anal. Bioanal. Chem 2009, 395 (3), 829–837. [PubMed: 19685340]

(28). De Sa Peixoto P; Laurent G; Azaïs T; Mosser G Solid-State NMR Study Reveals Collagen I Structural Modifications of Amino Acid Side Chains upon Fibrillogenesis. J. Biol. Chem 2013, 288 (11), 7528–7535. [PubMed: 23341452]

(29). Bazrafshan Z; Stylios GK A Novel Approach to Enhance the Spinnability of Collagen Fibers by Graft Polymerization. Mater. Sci. Eng., C 2019, 94, 108–116.

(30). bmse000966 Trans 4 Hydroxy-L-proline at BMRB. http://bmrb.wisc.edu/metabolomics/mol_summary/show_data.php?id=bmse000966 (accessed Mar 30, 2020).

(31). Wishart DS; Knox C; Guo AC; Eisner R; Young N; Gautam B; Hau DD; Psychogios N; Dong E; Bouatra S; Mandal R; Sinelnikov I; Xia J; Jia L; Cruz JA; Lim E; Sobsey CA; Shrivastava S; Huang P; Liu P; Fang L; Peng J; Fradette R; Cheng D; Tzur D; Clements M; Lewis A; De Souza A; Zuniga A; Dawe M; Xiong Y; Clive D; Greiner R; Nazyrova A; Shaykhutdinov R; Li L; Vogel HJ; Forsythe I HMDB: A Knowledgebase for the Human Metabolome. Nucleic Acids Res. 2009, 37, D603–D610. [PubMed: 18953024]

(32). bmse000966 Trans 4 Hydroxy-L-proline at BMRB. http://bmrb.wisc.edu/metabolomics/mol_summary/show_data.php?id=bmse000966 (accessed Mar 30, 2020).

(33). de Campos Vidal B; Mello MLS Collagen Type I Amide I Band Infrared Spectroscopy. Micron 2011, 42, 283–289. [PubMed: 21134761]

(34). Payne KJ; Veis A Fourier Transform Ir Spectroscopy of Collagen and Gelatin Solutions: Deconvolution of the Amide I Band for Conformational Studies. Biopolymers 1988, 27, 1749–1760. [PubMed: 3233328]

(35). Kong J; Yu S Fourier Transform Infrared Spectroscopic Analysis of Protein Secondary Structures. Acta Biochim. Biophys. Sin 2007, 39, 549–559. [PubMed: 17687489]

(36). Doyle BB; Bendit EG; Blout ER Infrared Spectroscopy of Collagen and Collagen-like Polypeptides. Biopolymers 1975, 14, 937–957. [PubMed: 1156652]

(37). Dzierwa A; Reizer R; Pawlus P; Grabon W Variability of Areal Surface Topography Parameters due to the Change in Surface Orientation to Measurement Direction. Scanning 2014, 36, 170–183. [PubMed: 23878095]

(38). Olympus. Surface Roughness Measurement—Evaluating Parameters Contáctenos Obtenga una cotización. https://www.olympus-ims.com/es/metrology/surface-roughness-measurement-portal/evaluating-parameters/.

(39). Callister WD Jr.; Rethwisch DG Fundamentals of Materials Science and Engineering: An Integrated Approach; John Wiley & Sons, 2012.

(40). Slater K; Partridge J; Nandivada H Tuning the Elastic Moduli of Corning Matrigel and Collagen I 3D Matrices by Varying the Protein Concentration; Application Note, Corning, 2017.

(41). Golatta M; Schweitzer-Martin M; Harcos A; Schott S; Junkermann H; Rauch G; Sohn C; Heil J Normal Breast Tissue Stiffness Measured by a New Ultrasound Technique: Virtual Touch Tissue Imaging Quantification (VTIQ). Eur. J. Radiol 2013, 82 (11), e676–e679. [PubMed: 23932637]

(42). Guimarães CF; Gasperini L; Marques AP; Reis RL The Stiffness of Living Tissues and Its Implications for Tissue Engineering. Nature Reviews Materials. 2020, 5, 351.

(43). Skardal A; Mack D; Atala A; Soker S Substrate Elasticity Controls Cell Proliferation, Surface Marker Expression and Motile Phenotype in Amniotic Fluid-Derived Stem Cells. J. Mech. Behav. Biomed. Mater 2013, 17, 307–316. [PubMed: 23122714]

(44). Griesenauer RH; Weis JA; Arlinghaus LR; Meszoely IM; Miga MI Breast Tissue Stiffness Estimation for Surgical Guidance Using Gravity-Induced Excitation. Phys. Med. Biol 2017, 62 (12), 4756–4776. [PubMed: 28520556]

(45). Piao J; You K; Guo Y; Zhang Y; Li Z; Geng L Substrate Stiffness Affects Epithelial-Mesenchymal Transition of Cervical Cancer Cells through miR-106b and Its Target Protein DAB2. Int. J. Oncol 2017, 50 (6), 2033–2042. [PubMed: 28498390]

(46). Saha S; Duan X; Wu L; Lo P-K; Chen H; Wang Q Electrospun Fibrous Scaffolds Promote Breast Cancer Cell Alignment and Epithelial-Mesenchymal Transition. Langmuir 2012, 28 (4), 2028–2034. [PubMed: 22182057]

(47). Chang M Tamoxifen Resistance in Breast Cancer. Biomol. Ther 2012, 20 (3), 256–267.

(48). Chen S-H; Hei Antonio Cheung C Challenges in Treating Estrogen Receptor-Positive Breast Cancer. Estrogen. 2019, DOI: 10.5772/intechopen.79263.

(49). Rocca A; Maltoni R; Bravaccini S; Donati C; Andreis D Clinical Utility of Fulvestrant in the Treatment of Breast Cancer: A Report on the Emerging Clinical Evidence. Cancer Manage. Res 2018, 10, 3083–3099.

(50). Jordan VC Tamoxifen (ICI46,474) as a Targeted Therapy to Treat and Prevent Breast Cancer. Br. J. Pharmacol 2006, 147, S269–S276. [PubMed: 16402113]

(51). Tannock IF; Lee CM; Tunggal JK; Cowan DSM; Egorin MJ Limited Penetration of Anticancer Drugs through Tumor Tissue: A Potential Cause of Resistance of Solid Tumors to Chemotherapy. Clin. Cancer Res 2002, 8 (3), 878–884. [PubMed: 11895922]

(52). Januchowski R; Zawierucha P; Ruciński M; Nowicki M; Zabel M Extracellular Matrix Proteins Expression Profiling in Chemoresistant Variants of the A2780 Ovarian Cancer Cell Line. Biomed Res. Int 2014, 2014, 365867. [PubMed: 24804215]

(53). Talukdar S; Kundu SC A Non-Mulberry Silk Fibroin Protein Based 3D In Vitro Tumor Model for Evaluation of Anticancer Drug Activity. Adv. Funct. Mater 2012, 22, 4778–4788.

(54). Herrmann D; Conway JRW; Vennin C; Magenau A; Hughes WE; Morton JP; Timpson P Three-Dimensional Cancer Models Mimic Cell-Matrix Interactions in the Tumour Microenvironment. Carcinogenesis 2014, 35, 1671–1679. [PubMed: 24903340]

(55). Sethi T; Rintoul RC; Moore SM; MacKinnon AC; Salter D; Choo C; Chilvers ER; Dransfield I; Donnelly SC; Strieter R; Haslett C Extracellular Matrix Proteins Protect Small Cell Lung Cancer Cells against Apoptosis: A Mechanism for Small Cell Lung Cancer Growth and Drug Resistance in Vivo. Nat. Med 1999, 5 (6), 662–668. [PubMed: 10371505]

(56). Januchowski R;Świerczewska M; Sterzyńska K; Wojtowicz K; Nowicki M; Zabel M Increased Expression of Several Collagen Genes Is Associated with Drug Resistance in Ovarian Cancer Cell Lines. J. Cancer 2016, 7, 1295–1310. [PubMed: 27390605]

(57). Gullberg DE; Lundgren-Åkerlund E Collagen-Binding I Domain Integrins — What Do They Do? Prog. Histochem. Cytochem 2002, 37, 3–54. [PubMed: 11876085]

(58). Nissinen L; Koivunen J; Käpylä J; Salmela M; Nieminen J; Jokinen J; Sipilä K; Pihlavisto M; Pentikäinen OT; Marjamäki A; Heino J Novel $\alpha 2\beta 1$ Integrin Inhibitors Reveal That Integrin Binding to Collagen under Shear Stress Conditions Does Not Require Receptor Preactivation. J. Biol. Chem 2012, 287, 44694–44702. [PubMed: 23132859]

(59). Xu B; Lefringhouse J; Liu Z; West D; Baldwin LA; Ou C; Chen L; Napier D; Chaiswing L; Brewer LD; St. Clair D; Thibault O; van Nagell JR; Zhou BP; Drapkin R; Huang J-A; Lu ML; Ueland FR; Yang XH Inhibition of the integrin/FAK Signaling Axis and c-Myc Synergistically Disrupts Ovarian Cancer Malignancy. Oncogenesis 2017, 6 (1), e295. [PubMed: 28134933]

(60). Yu H; Gao M; Ma Y; Wang L; Shen Y; Liu X Inhibition of Cell Migration by Focal Adhesion Kinase: Time-Dependent Difference in Integrin-Induced Signaling between Endothelial and Hepatoblastoma Cells. Int. J. Mol. Med 2018, 41 (5), 2573–2588. [PubMed: 29484384]

(61). Tancioni I; Uryu S; Sulzmaier FJ; Shah NR; Lawson C; Miller NLG; Jean C; Chen XL; Ward KK; Schlaepfer DD FAK Inhibition Disrupts a β5 Integrin Signaling Axis Controlling Anchorage-Independent Ovarian Carcinoma Growth. Mol. Cancer Ther 2014, 13 (8), 2050–2061. [PubMed: 24899686]

(62). Koizume S; Miyagi Y Breast Cancer Phenotypes Regulated by Tissue Factor-Factor VII Pathway: Possible Therapeutic Targets. World J. Clin. Oncol 2014, 5 (5), 908–920. [PubMed: 25493229]

(63). Guo L; Wang J; Zhang T; Yang Y Glypican-5 Is a Tumor Suppressor in Non-Small Cell Lung Cancer Cells. Biochem Biophys Rep 2016, 6, 108–112. [PubMed: 27092337]

(64). Yang X; Zhang Z; Qiu M; Hu J; Fan X; Wang J; Xu L; Yin R Glypican-5 Is a Novel Metastasis Suppressor Gene in Non-Small Cell Lung Cancer. Cancer Lett. 2013, 341 (2), 265–273. [PubMed: 23962560]

(65). Wallner C; Drysch M; Becerikli M; Jaurich H; Wagner JM; Dittfeld S; Nagler J; Harati K; Dadras M; Philippou S; Lehnhardt M; Behr B Interaction with the GDF8/11 Pathway Reveals Treatment Options for Adenocarcinoma of the Breast. Breast 2018, 37, 134–141. [PubMed: 29156385]

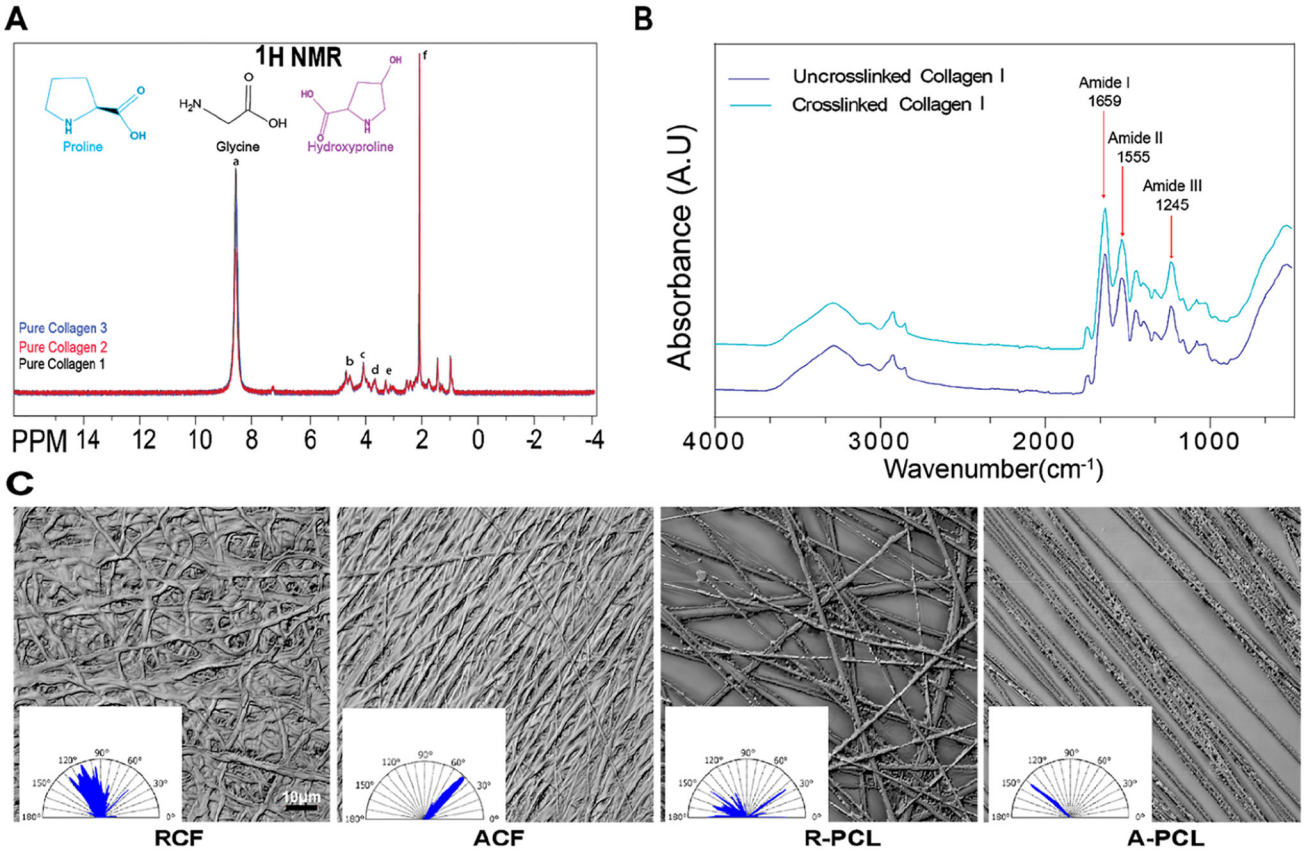


**Figure 1.**

Physical and chemical characterization of culture substrates. (A) Overlapped $^{1}$H NMR spectra of commercial type I collagen to confirm molecular composition across three independent batches. (B) FTIR spectra of uncross-linked and cross-linked collagen I. (C) Representative images of the organization of random (RCF) and aligned (ACF) collagen fibrils and random (R-PCL) and aligned (A-PCL) polycaprolactone fibers, with their respective angle spectrum. The angle spectrum was used to calculate the Str parameter shown in Table 1. Data in A and B represent the means of three independent batches of substrates with $n = 3$.

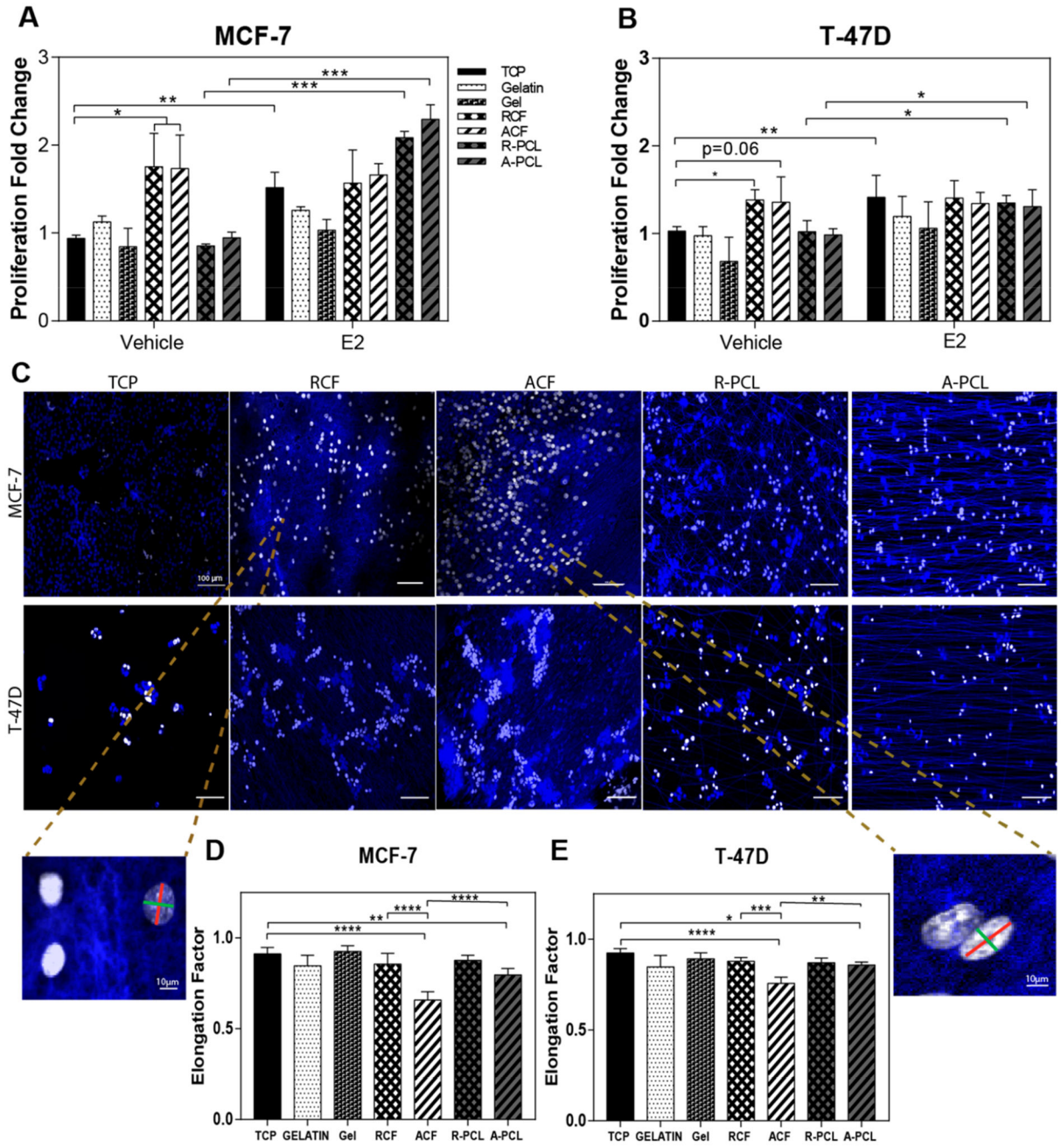


**Figure 2.**

Collagen fibrous substrates support tumor cell proliferation in a hormone-restricted culture. Effects of substrate composition and orientation on MCF-7 and T-47D cells. (A,B) MCF-7 and T-47D cells were cultured in hormone-depleted conditions ± the estradiol (E2) ligand (1 nM) on tissue culture plastic (TCP), gelatin coating on TCP (gelatin), collagen gel (gel), RCF, ACF, R-PCL, and A-PCL. Proliferation data represent the average % of EdU positive cells, as determined by flow cytometry, normalized to TCP. Data represent the average mean ± SE of three independent experiments with $n = 3$. (C) Representative fluorescent images of nonestrogen treated MCF-7 and T-47D cells stained with Hoescht and EdU-Alexa 488

to label the nucleus (blue) and cells in the S phase (white), respectively, using confocal microscopy. The white scale bar represents 100 $\mu$m. (D,E) Elongation factor (nucleus elongation) of nonestrogen treated MCF-7 and T-47D cells, represented as the ratio of the minor (green line) and major (red line) axes of the nucleus. Data represent the average mean ± SE of three independent experiments with $n = 4$; *$p < 0.05$, **$p < 0.01$, ***$p < 0.001$, and ****$p < 0.0001$.

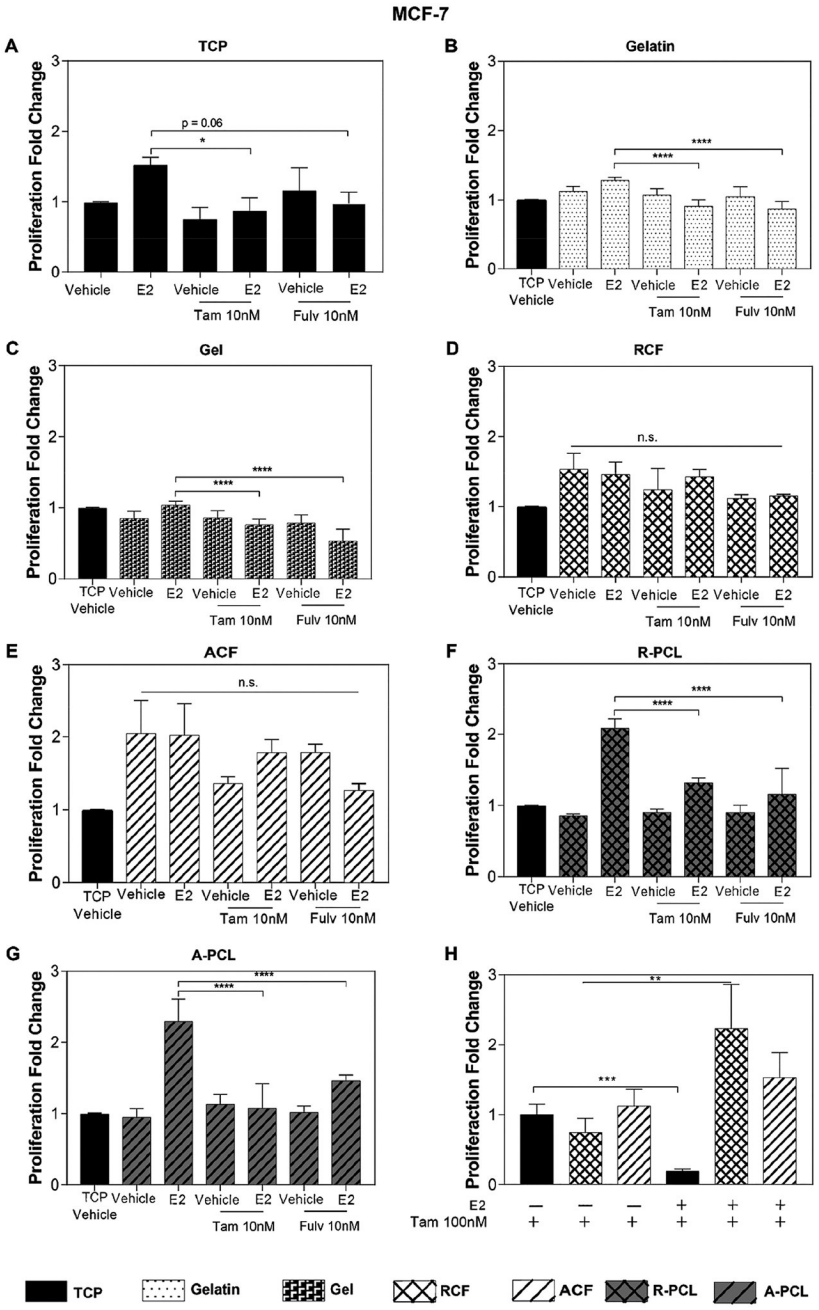


**Figure 3.**

MCF-7 sensitivity to ER inhibitors. (A–G) Proliferation analysis of the MCF-7 cells treated with 1 nM of E2 and 10 nM Tamoxifen and 10 nM of Fulvestrant cultured on (A) TCP, (B) gelatin, (C) collagen I gel, (D) RCF, (E) ACF, (F) R-PCL, and (G) A-PCL substrates. (H) Proliferation analysis of MCF-7 cells treated with 1 nM of E2 and 100 nM of Tamoxifen on TCP, RCF, and ACF; data are relative to TCP without estrogen and with Tam100 nM. Data represent the average of three to four independent experiments with $n = 3–4$, SE, $*p < 0.05$, $**p < 0.01$, $***p < 0.001$, and $****p < 0.0001$, presented as the fold change relative to the TCP substrate without estrogen (vehicle) shown in graph A.

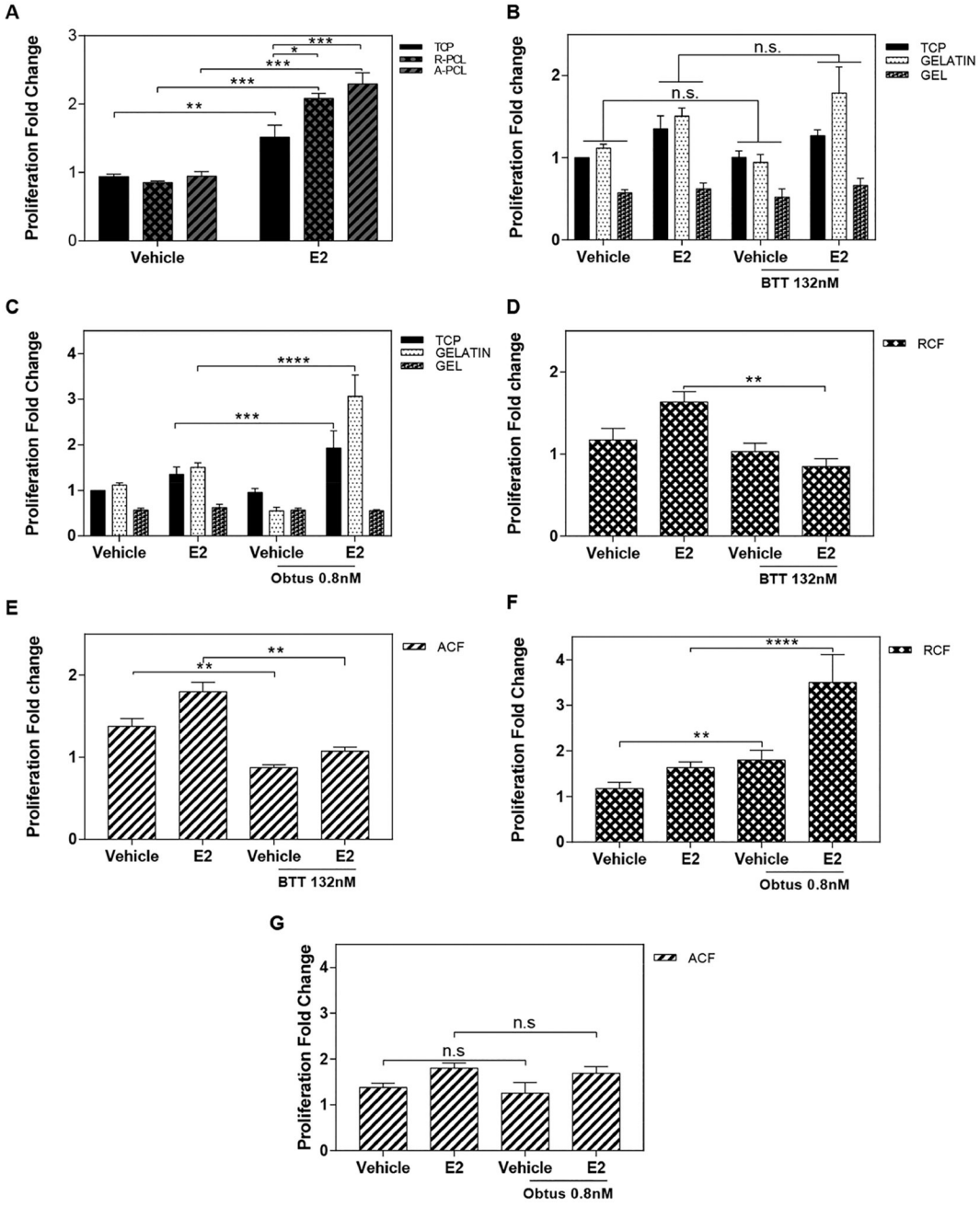


**Figure 4.**

Impact of $\alpha 2\beta 1$ and $\alpha 1\beta 1$ integrin signaling on collagen fibril-stimulated cell proliferation. (A) Proliferation analysis of the MCF-7 cells on nonintegrin-binding substrates (TCP and PCL). (B,C) Proliferation analysis of the MCF-7 cells cultured ± estradiol ligand (E2) and treated with BTT 3033 132 nM ($\alpha_2\beta_1$ integrin inhibitor) on TCP, gelatin and collagen gel (B), RCF (C), and ACF (D). (E) Proliferation analysis of the MCF-7 cells cultured ± estradiol ligand (E2) and treated with 0.8 nM Obtustatin ($\alpha_1\beta_1$ integrin inhibitor) on TCP, gelatin and collagen gel (A), RCF (B), and ACF (C). (E) Proliferation analysis of the MCF-7 cells cultured ± estradiol ligand (E2) and treated with 0.8 nM Obtustatin ($\alpha 1\beta 1$ integrin

inhibitor) on TCP, gelatin and collagen gel (E), RCF (F), and ACF (G). Data represent the mean of three to four independent experiments with $n = 3–4$, SE, $^{*}p < 0.05$, $^{**}p < 0.01$, $^{***}p < 0.001$, and $^{****}p < 0.0001$.

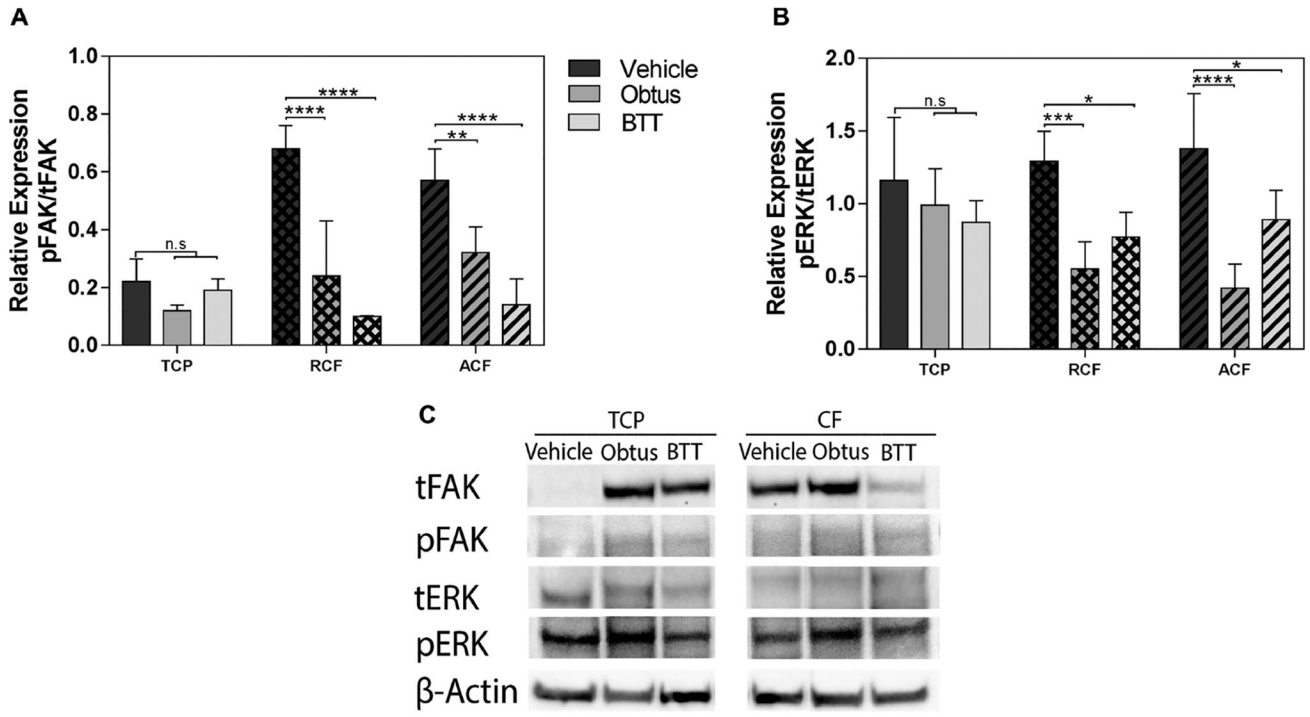


**Figure 5.**

FAK and ERK signaling activity. Quantification of relative expression of total focal adhesion kinase (tFAK; 119 kDa) and phosphorylated FAK (pFAK; 119 kDa), total extracellular-signal-regulated kinase (tERK; 42–44 kDa), and phosphorylated ERK (pERK; 42–44 kDa) in tumor cells relative to $\beta$-actin (42 kDa). Quantification of (A) pFAK in tFAK expression and (B) pERK in tERK by image analysis of the Western blots bands. Data represent the relative mean intensity ± standard error of three independent experiments. (C) Representative protein bands are shown for TCP and collagen fibrils (CF).

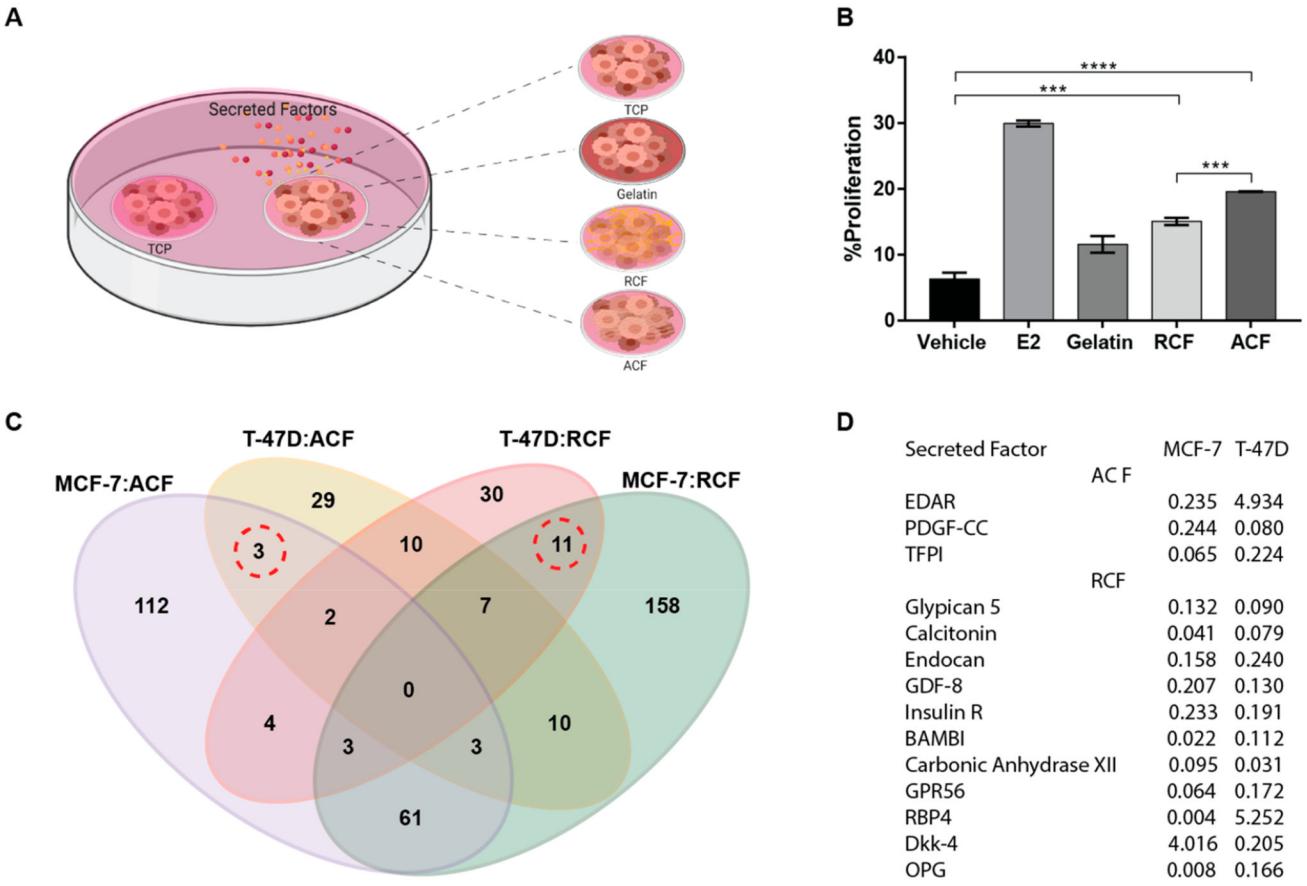


D

| Secreted Factor | MCF-7 | T-47D |
|---|---|---|
| ACF | | |
| EDAR | 0.235 | 4.934 |
| PDGF-CC | 0.244 | 0.080 |
| TFPI | 0.065 | 0.224 |
| RCF | | |
| Glypican 5 | 0.132 | 0.090 |
| Calcitonin | 0.041 | 0.079 |
| Endocan | 0.158 | 0.240 |
| GDF-8 | 0.207 | 0.130 |
| Insulin R | 0.233 | 0.191 |
| BAMBI | 0.022 | 0.112 |
| Carbonic Anhydrase XII | 0.095 | 0.031 |
| GPR56 | 0.064 | 0.172 |
| RBP4 | 0.004 | 5.252 |
| Dkk-4 | 4.016 | 0.205 |
| OPG | 0.008 | 0.166 |

**Figure 6.**

Soluble factor-mediated effect and secretome profile. (A) Schematic of a two-microwell array made of polystyrene was used to evaluate the effect of cell–substrate interactions on adjacent cultures. (B) Proliferation analysis of MCF-7 cells seeded on TCP adjacent to MCF-7 cells on gelatin, RCF, or ACF after 72 h. Data represent the mean of four independent experiments with $n = 3–5 \pm$ SE, *$p < 0.05$, **$p < 0.01$, ***$p < 0.001$, and ****$p < 0.0001$. (C) Secreted proteins in conditioned media that are differentially expressed in MCF-7 and T47D relative to TCP. Quantitative analysis of the expression levels of 640 proteins in conditioned media using the human quantitative proteomics array (RayBiotech). MCF-7 cells were seeded on TCP, RCF, and ACF. Conditioned media were collected at 72 h after cell seeding. The logical overlap of upregulated or downregulated secreted factors by ±4 fold across different substrates is shown in the Venn diagram. (D) Table of secreted factors expressed by both MCF-7 and T47D but differentially expressed (marked by dotted lines in 5C) by a 4-fold change or higher in aligned or random substrates as compared to TCP.

**Table 1.**

Physical and Mechanical Characterization of Culture Substrates

| substrate | fiber diameter ($\mu$m) | Str (ratio)[a] | stiffness (kPa) |
|---|---|---|---|
| TCP | | 0.543 ± 0.075 | $3.8 \times 10^6 \pm 0.9 \times 10^6$ |
| gelatin thin coating on TCP | | 0.651 ± 0.026 | $2.4 \times 10^6 \pm 0.8 \times 10^6$ |
| collagen gel | | 0.551 ± 0.0096 | 0.00754 ± 0.0015 |
| RCF | 0.35 ± 0.17 | 0.496 ± 0.006 | 13.2 ± 2.4 |
| ACF | 0.33 ± 0.13 | 0.201 ± 0.079 | 14.3 ± 3.5 |
| R-PCL | 1.001 ± 0.261 | 0.291 ± 0.063 | 15.9 ± 3.5 |
| A-PCL | 1.05 ± 0.153 | 0.06 ± 0.0051 | 15.8 ± 1.2 |

[a]Str values represent a texture aspect ratio. Values have an inverse correlation with the uniformity of the surface texture. Data represent the means of three to six independent batches of substrates with $n = 3–10 \pm$ SE. Substrates: Tissue culture plastic (TCP), random collagen fibrils (RCF), aligned collagen fibrils (ACF), random polycaprolactone fibers (R-PCL), and aligned polycaprolactone fibers (A-PCL).